Materials Transactions, Vol. 48, No. 9 (2007) pp. 2370 to 2373

Structural Analysis of Polycrystalline $BiFeO_3$ Films by Transmission Electron Microscopy

Hiroshi Naganuma[1], Andras Kovacs[2], Akihiko Hirata[2], Yoshihiko Hirotsu[2] and Soichiro Okamura[1]

[1]*Department of Applied Physics, Faculty of Science, Tokyo University of Science, Tokyo 162-8601, Japan*
[2]*The Institute of Scientific and Industrial Research, Osaka University, Osaka 567-0047, Japan*

A multiferroic polycrystalline $BiFeO_3$ film has been fabricated by a chemical solution deposition followed by the post deposition annealing at 823 K in air. The nanostructure of the $BiFeO_3$ film was characterized by transmission electron microscopy (TEM). The nano-beam electron diffraction and the fast Fourier transform pattern image from the high resolution TEM image were compared with the electron diffraction patterns of the multislice simulation, and it was revealed that the $BiFeO_3$ has *R*3*c* rhombohedral structure. Formation of any additional phase or phases was not found in the sample. The $BiFeO_3$ film shows the small saturation magnetization of 5.2 emu/cm^3 without spontaneous magnetization at room temperature, which behavior is typical for the weak ferromagnetic materials. The ferroelectric hysteresis loop of the $BiFeO_3$ film was measured at low temperature in order to reduce the leakage current. The remanent polarization and the electric coercive field at 90 K were 52 μC/cm^2 and 0.51 MV/cm at an applied electric field of 1.4 MV/cm, respectively. The structure-magnetic properties relationship is also discussed. [doi:10.2320/matertrans.MAW200782]

(Received April 25, 2007; Accepted June 14, 2007; Published August 25, 2007)

Keywords: *multiferroics, bismuth iron oxide film, transmission electron microscopy, crystal structure, magnetic properties, ferroelectric properties*

1. Introduction

A multiferroic $BiFeO_3$ material has attracted much attention recently due to the coexistence of the ferroelectric and the magnetic order parameters.[1)] The $BiFeO_3$ shows the high ferroelectric ($T_C \sim 1100$ K)[2–4)] and the magnetic ($T_N \sim 650$ K)[5–7)] transition temperature. In the case of the ferroelectricity, the high remanent polarizations were reported recently in the film specimen, though the values were ranging from 50 and 150 μC/cm^2. [Ref. 1), 8), 9)] According to the first principle calculation,[10,12)] the spontaneous polarization of $BiFeO_3$ changes due to the crystal structure either rhombohedral or tetragonal. The tetragonal structure of the $BiFeO_3$ (SG: *P*4*mm*) should possess the spontaneous polarization of around 150 μC/cm^2 and the rhombohedral structure (SG: *R*3*c*) shows around 100 μC/cm^2 along the [111] direction without strains.[10,12)] A few percents of the strains is also affected to the spontaneous polarization in each crystal structure.[11,12)] Therefore, it is necessary to investigate not only the crystal structure but also the strain of the lattice, when discussing the remanent polarization of the $BiFeO_3$. On the contrary, the magnetic moments of iron atoms in the $BiFeO_3$ are coupled ferromagnetically within the pseudocubic (111) planes and antiferromagnetically between adjacent planes and the iron magnetic moments are slightly canting, which lead to the weak ferromagnetism.[13)] Actually, the $BiFeO_3$ shows almost no spontaneous magnetization as well as magnetic coercive field and the shape of the magnetic hysteresis loops is a typical for the weak ferromagnetic materials. However, the saturation magnetization of $BiFeO_3$ was different in each report.[14,15)] The differences may be attributed to the formation of the secondary phase, such as superparamagnetic nanoparticles consisted of the iron oxide, because the magnetic hysteresis loop of the superparamagnetism does not exhibit the spontaneous magnetization; therefore if the iron oxide superparamagnetic nanoparticles are formed, the saturation magnetization increases without drastic change of the shape of the magnetic hysteresis loop. Thus, there is a possibility that the $BiFeO_3$ film with high saturation magnetization include the superparamagnetic nanoparticles. It is difficult to detect such a small size of the nanoparticles inside of the film using a conventional X-ray diffraction measurement. A transmission electron microscopy (TEM) observation is effective to investigate such a small size of iron oxide superparamagnetic nanoparticle.

In this study, we fabricated the $BiFeO_3$ polycrystalline film by chemical solution deposition (CSD) followed by the post deposition annealing at 823 K in air and observed the structure of $BiFeO_3$ polycrystalline film by TEM. The rhombohedral structure of $BiFeO_3$ was confirmed by detailed TEM analyses and by multislice simulations of electron diffraction patterns. The ferroelectric and the magnetic prosperities of the $BiFeO_3$ film were also measured, as described in the following section.

2. Experimental Procedure

$BiFeO_3$ films were fabricated by the CSD method onto Pt/Ti/SiO_2/Si(100) substrate followed by the post-deposition annealing at 823 K for 10 min in air. After annealing, a top Pt electrode layer was deposited by an r.f. magnetron sputtering at room temperature. The film thickness of the $BiFeO_3$ film was 263 nm. Structure of the sample was determined by cross-sectional TEM observation using a JEOL JEM-3000F microscope working at 300 kV as well as the conventional $\theta/2\theta$ X-ray diffraction measurement. The local structure of $BiFeO_3$ layer was analyzed by nano-beam diffraction patterns (NBD). The NBDs were taken with beam size of ~4 nm. The electron energy-loss spectroscopy (EELS) analysis was carried out by a LEO-922 microscope equipped with Ω-type energy filter. The three-window technique was applied to get the net element-selective image. The ferro-

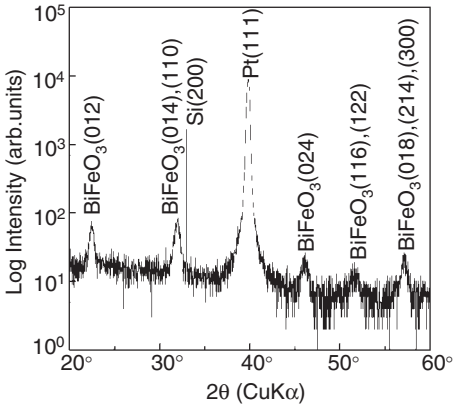

Fig. 1 X-ray diffraction pattern for the $BiFeO_3$ film annealing at 823 K in air.

electric hysteresis loops were performed by making use of ferroelectric tester (aixACCT TF-2000) with a single triangular pulse of 1 kHz at 90 K. Driving voltage was applied to the bottom electrode. Magnetic properties were measured at room temperature by a superconducting quantum interference device (SQUID) magnetometer (MPMS-XL) with the maximum applied magnetic field of ±5 Tesla to the in plane direction.

3. Results and Discussion

Figure 1 shows the X-ray diffraction pattern for the $BiFeO_3$ film annealing at 823 K in air before the upper Pt electrode deposition. The strong Pt(111) diffraction peak indicate the strong 111 texture of bottom Pt electrode layer. Other diffraction peaks were attributed to the $BiFeO_3$ structure, even though the apparent split of the neighboring diffraction peak could not be observed. No indication of other phase appearance in the XRD spectrum, meaning that the single phase of the polycrystalline $BiFeO_3$ film formed. Obvious shift of the diffraction peaks was not observed, implying that the layer does not have remarkable strain along the substrate normal.

In our previous study, the high leakage current density was observed in the $BiFeO_3$ film.[16] Note that difficult to measure accurately the ferroelectric hysteresis loops of the material with the high leakage current density, because the leakage current is also summarized with polarization reversal current. One of the ways to reduce the component of leakage current density is decreasing the measuring temperature. Actually, the leakage current density of the $BiFeO_3$ film drastically decreased by dropping the temperature (not shown). Therefore, in the present study, the ferroelectric hysteresis loop was measured at low temperature. Figure 2(a) shows the *P-E* hysteresis loop of the $BiFeO_3$ film measured at 90 K using a triangular wave form of 1 kHz. The remanent polarization and the electric coercive field of the $BiFeO_3$ film were 52 μC/cm^2 and 0.51 MV/cm, respectively. The remanent polarization of the present $BiFeO_3$ film is much higher than that of the remanent polarization of the bulk[17] but lower than that of the theoretical value.[18] Figure 2(b) shows the magnetization curve at room temperature of the $BiFeO_3$ film. Magnetization

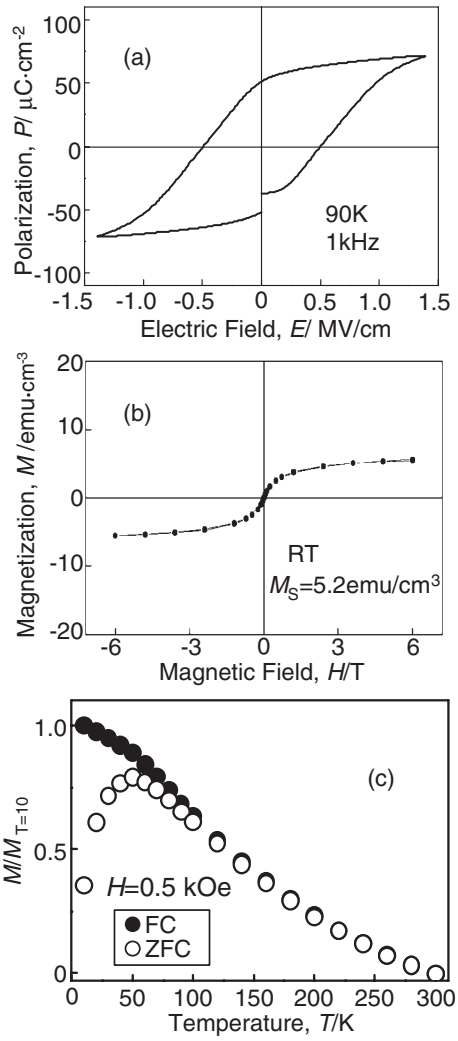

Fig. 2 *P-E* hysteresis loop measured at 90 K using a triangular wave form of 1 kHz (a), magnetization curve at room temperature (b) and FC-ZFC curves (c) for the $BiFeO_3$ film.

curve showed the low saturation magnetization of around 5.2 emu/cm^3 together with the no spontaneous magnetization as well as the magnetic coercive field. Figure 2(c) shows the field-cooling, zero-field cooling (FC-ZFC) curves for the $BiFeO_3$ film. The applied magnetic field during the FC-ZFC measurement was 0.5 kOe. Magnetization monotonically decreased as the temperature increased in FC curve, though the broad peak was appeared at around 50 K in the ZFC curve, indicating the possible presence of the superparamagnetic nanoparticles. According to our previous study,[16] the broad peak in the ZFC curve was appeared at 70 K under the applied magnetic field of 0.2 kOe, suggesting that the broad peak was shifted by the magnitude of the applied magnetic field.

The detailed structure analysis of the polycrystalline $BiFeO_3$ film was carried out by TEM observation. Figure 3 show the cross sectional bright-field (BF) TEM images of Pt/$BiFeO_3$/Pt interfaces. The relatively smooth interface was formed at the upper side of the Pt electrode. On the contrary, a thin interfacial layer was formed between the bottom side of the Pt electrode and $BiFeO_3$ layers with the thickness of around 1–2 nm as shown in the TEM image. The high

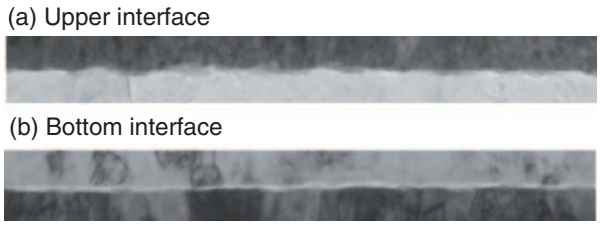

Fig. 3 Cross sectional bright-field TEM images of Pt/$BiFeO_3$/Pt interfaces.

resolution TEM observation revealed that the interfacial layer has an amorphous structure.[19] To investigate the composition of the amorphous interfacial layer as well as the compositional homogeneity of the film, we measured an EELS elemental mapping of the $BiFeO_3$ film.

Figure 4 shows cross sectional EELS elemental mappings of iron and oxygen obtained using the three-window method, together with a corresponding bright field TEM image. The iron- and oxygen-mapping images were taken by using Fe *L*- and O *K*-edges, respectively. The apparent inhomogeneous contrast could not be observed in both iron and oxygen elemental mapping images, indicating that there is no obvious segregation of Fe and O in the film. Note that the fine slight contrasts were probably ascribed to the remains of the diffraction contrast. At the interface of the bottom Pt electrode, no clear difference of the contrast was observed due to the spatial resolution of the TEM. Therefore, the composition of the amorphous interfacial layer was unclear at this moment. In terms of the ferroelectric properties, the thin amorphous layer seems to be not strongly affected to the ferroelectricity because the shape of the ferroelectric hysteresis loop measured at 90 K was symmetric belong to the electric field.

Figure 5 show a high resolution TEM image and the corresponding fast Fourier transform pattern image 5(a) and an NBD pattern 5(b) and the simulated electron diffraction pattern 5(c). The high resolution TEM image contains periodic lattice fringes along the [012] direction and their spacings are approximately 0.396 nm which is in good agreement with the Kubel's report.[20] The electron diffraction pattern was simulated by the MacTEMPAS computer

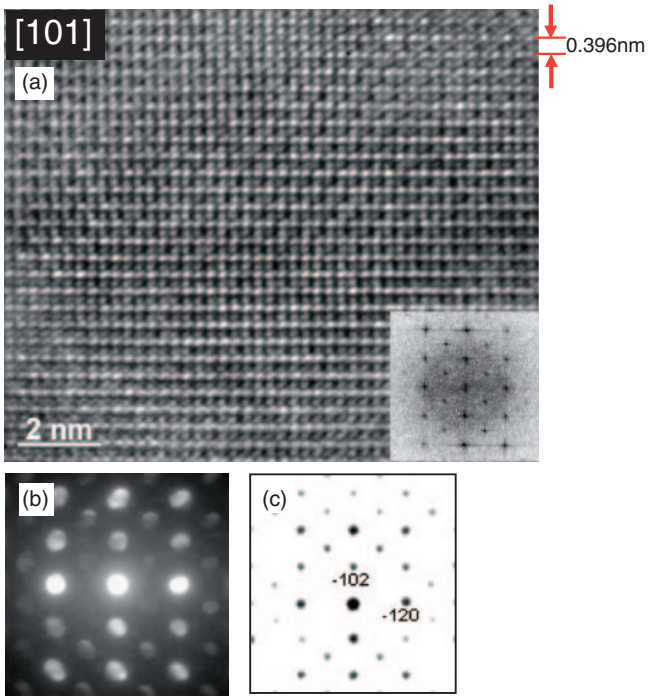

Fig. 5 High resolution TEM image and the corresponding fast Fourier transform pattern image (a) and an NBD pattern (b) and the simulated electron diffraction pattern (c).

program applying the multislice method[21] and using the structure data of rhombohedral *R*3*c* and of tetragonal *Pbmm* lattices.[1,14,20] In comparison of the simulated electron diffractions with the NBD pattern it was found that the $BiFeO_3$ layer has rhombohedral *R*3*c* structure.

As mentioned above, the broad peak was observed at 50 K in the ZFC curve under the applied magnetic field of 0.5 kOe. When comparing the case of the applied magnetic filed of 0.2 kOe,[16] the peak position was shifted to the lower temperature. In the case of the superparamagnetic system, the blocking temperature increased as the applied magnetic field increased for the systems of the noninteracting superparamagnetic particles,[22] while the blocking temperature decreased for the interacting systems.[23] Our specimen should be the interacting system, even though it is difficult to directly referring these system to our case due to the $BiFeO_3$ matrix of

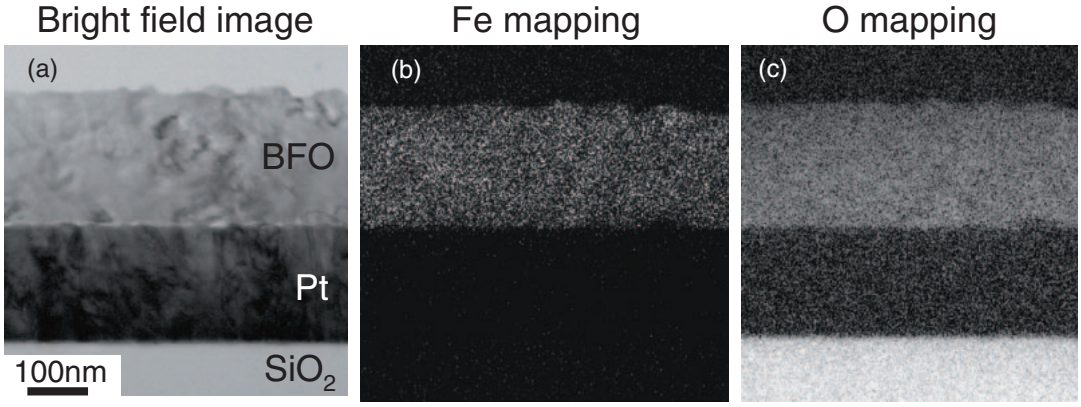

Fig. 4 Cross sectional bright field TEM image (a) and corresponding EELS elemental mappings of iron (b) and oxygen (c) obtained using the three-window method.

the weak ferromagnetism. The interacting system seems to be the superparamagnetic nanoparticles with high density, though such a kind of nanoparticles could not be found through the TEM observation in our $BiFeO_3$ film. Thus, it could be considered that the broad peak in the ZFC curved is not attributed to the superparamagnetic nanoparticles. On the other hand, the amorphous $BiFeO_3$ behave as spin glassy and the broad peak was observed at around 20 K under the magnetic field of 0.2 kOe.[24] In our experiment the TEM analysis did not show the any formation of amorphous phase, except the interfacial amorphous layer. Although the magnetic property of the interfacial amorphous layer was not revealed yet, 1~2 nm-thick of the interfacial amorphous layer is too thin to affect the macroscopic magnetic properties, even if the interfacial amorphous layer behaves like spin glass. In order to understand the spin glassy behavior in $BiFeO_3$ film, further investigation using the AC susceptibility measurement and/or the applied magnetic field dependence of the broad peak position in the ZFC curve is necessary to verify this hypothesis. The remanent polarization at 90 K was around 52 $\mu C/cm^2$, which is much higher than that of the bulk remanent polarization of around 3.5 $\mu C/cm^2$.[16] Although it can not directly be compared to the theoretical prediction value due to the polycrystalline structure of the present $BiFeO_3$ film, around 52 $\mu C/cm^2$ of the remanent polarization is low. However, it is clear that the $BiFeO_3$ material should possess the high remanent polarization even though rhombohedral *R*3c structure without any effective structural strains.

4. Conclusion

We fabricated the $BiFeO_3$ film on the $Pt/Ti/SiO_2/Si(100)$ substrate by the CSD method and characterized their structures using TEM observation. The TEM observation revealed that the rhombohedral *R*3*c* structured polycrystalline $BiFeO_3$ film was formed in our experiment. No remarkable strain and no indication of formation the other phase than $BiFeO_3$ were found. The relatively high remanent polarization of 52 $\mu C/cm^2$ at 90 K was obtained in the polycrystalline $BiFeO_3$ film. The remanent polarization is almost ten times higher than that of the bulk value though half of the theoretical prediction of the *R*3c structure. The low remanent polarization compared with the theoretical value could be responsible for the polycrystalline structure. The saturation magnetization was around 5.2 emu/cm^3 at room temperature without the spontaneous magnetization as well as the magnetic coercive field. The origin of the broad peak in ZFC curve is unclear; therefore further investigation is necessary to understand the cause of the broad peak.

Acknowledgments

Author A.K. on leave from Research Institute for Technical Physics and Materials Science, Budapest, Hungary. This study was partly funded by the Grant-in-Aid for Young Scientist [Start up program] (Grant No. 18860070) from the Ministry of Education, Culture, Sports, Science and Technology of Japan, and by the Sasakawa Scientific Research Grant from The Japan Society (Grant No. 19-216).

REFERENCES

1) J. Wang, J. B. Neaton, H. Zheng, V. Nagarajan, S. B. Ogale, B. Liu, D. Viehland, V. Vaithyanathan, D. G. Schlom, U. V. Waghmare, N. A. Spaldin, K. M. Rabe, M. Wuttig and R. Ramesh: Science **299** (2003) 1719.
2) Yu. N. Venevtsev, G. Zhadanow and S. Solov'ev: Sov. Phys. Crystallogr. **4** (1960) 538.
3) G. Smolenskii, V. Isupov, A. Agranovskaya and N. Krainik: Sov. Phys. Solid State **2** (1961) 2651.
4) Yu. E. Roginskaya, Yu. Ya. Tomashpol'skii, Yu. N. Venevtsev, V. M. Petrov and G. S. Zhdanov: Sov. Phys. JETP **23** (1966) 47.
5) G. Smolenskii, V. Yudin, E. Sher and Yu. E. Stolypin: Sov. Phys. JETP **16** (1963) 622.
6) S. V. Kiselev, R. P. Ozerov and G. S. Zhdanov: Sov. Phys. **7** (1963) 742.
7) P. Fischer, M. Polomskya, I. Sosnowska and M. Szymanksi: J. Phys. C **13** (1980) 1931.
8) J. Li, J. Wang, M. Wuttig, R. Ramesh, N. Wang, B. Ruette, A. P. Pyatakov, A. K. Zvezdin and D. Viehland: Appl. Phys. Lett. **84** (2004) 5261.
9) K. Y. Yun, D. Ricinschi, T. Kanashima and M. Okuyama: Applied Physics Lett. **89** (2006) 192902.
10) J. B. Neaton, C. Ederer, U. V. Waghmare, N. A. Spaidin and K. M. Rabe: Rhys. Rev. B **71** (2005) 014113.
11) C. Ederer and N. A. Spaldin: Phys. Rev. B **71** (2005) 224103.
12) C. Ederer and N. A. Spaldin: Phys. Rev. Lett. **95** (2005) 257601.
13) C. Ederer and N. A. Spaldin: Phys. Rev. B **71** (2005) 060401(R).
14) K. Y. Yun, M. Noda, M. Okuyama, H. Saeki, H. Tabata and K. Saito: J. Appl. Phys. **96** (2004) 3399.
15) Y. Wang, Q. Jiang, H. He and C. Nan: Appl. Phys. Lett. **88** (2006) 142503.
16) H. Naganuma and S. Okamura: J. Appl. Phys. **101** (2007) 09M103-1.
17) J. R. Teague, R. Gerson and W. J. James: Solic State Commun. **8** (1970) 1073.
18) J. B. Neaton, C. Ederer, U. V. Waghmare, N. A. Spaldin and K. M. Rabe: Phys. Rev. B **71** (2005) 014113.
19) H. Naganuma, A. Kovacs, Y. Hirotsu, Y. Inoue and S. Okamura: Trans. of the Mter. Res. Soc. of Jpn. **32**[1] (2007) 39.
20) F. Kubel and H. Schmid: Acta Cryst. B **46** (1990) 698.
21) E. J. Kirkland: *Advanced Computing in Electron Microscopy* (Plenum, New York, 1998).
22) W. Luo, S. R. Nagel, T. F. Rosenbaum and R. E. Rosensweig: Phys. Rev. Lett. **67** (1991) 2721.
23) M. Hanson, C. Johansson and S. Morup: J. Phys.: Condens. Matter **7** (1995) 9263.
24) S. Nakamura, S. Soeya, N. Ikeda and M. Tanaka: J. Appl. Phys. **74** (1993) 5652.